Inorganic Chemistry

Article

pubs.acs.org/IC

Topochemical Synthesis of Alkali-Metal Hydroxide Layers within Double- and Triple-Layered Perovskites

Dariush Montasserasadi,[†] Debasish Mohanty,[‡] Ashfia Huq,[§] Luke Heroux,[§] Edward Andrew Payzant,[§] and John B. Wiley*[,†]

[†]Department of Chemistry and the Advanced Materials Research Institute, University of New Orleans, 2000 Lakeshore Drive, New Orleans, Louisiana 70148-2820, United States

[‡]Materials Science and Technology Division, Oak Ridge National Laboratory, Oak Ridge, Tennessee 37831 United States

[§]Chemical and Engineering Materials Division, Oak Ridge National Laboratory, Oak Ridge, Tennessee 37831, United States

Supporting Information

ABSTRACT: The formation of alkali-metal hydroxide layers within lamellar perovskites has been accomplished by a two-step topochemical reaction strategy. Reductive intercalation of $ALaNb_2O_7$ with alkali metal (A = K, Rb) and $RbCa_2Nb_3O_{10}$ with Rb leads to $A_2LaNb_2O_7$ and $Rb_2Ca_2Nb_3O_{10}$, respectively. Oxidative intercalation with stoichiometric amounts of water vapor, produced by the decomposition of calcium oxalate monohydrate in a sealed ampule, allows the insertion hydroxide species. Compounds of the form $(A_2OH)LaNb_2O_7$ (A = K, Rb) and $(Rb_2OH)Ca_2Nb_3O_{10}$ are accessible. X-ray diffraction data indicates a clear layer expansion of almost 3 Å on the insertion of hydroxide relative to that of the parent. Rietveld refinement of neutron diffraction data collected on deuterated samples of $(Rb_2OD)LaNb_2O_7$ ($P4/mmm$ space group, a = 3.9348(1) Å, c = 14.7950(7) Å) finds that both rubidium and oxygen species reside in cubic sites forming a CsCl-like interlayer structure between niobate perovskite blocks. Hydrogens, attached to the interlayer oxygens, are disordered over a 4-fold site in the x–y plane and have O–H bond distances (0.98 Å) consistent with known hydroxide species. This synthetic approach expands the library of available topochemical reactions, providing a facile method for the construction of alkali-metal hydroxide layers within receptive perovskite hosts.

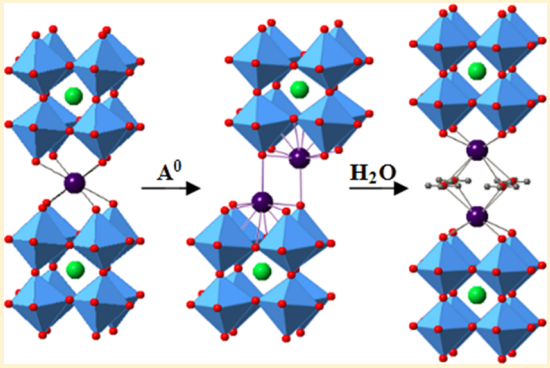

INTRODUCTION

Ion-exchangeable layered perovskites, which consist of perovskite slabs separated by interlayer cations, include the two major groups Dion–Jacobson (DJ) $A[A'_{n-1}B_nO_{3n+1}]$ and Ruddlesden–Popper (RP) $A_2[A'_{n-1}B_nO_{3n+1}]$,[1] where typically A = alkali metal, A′ = rare earth or alkaline-earth, B = transition metal, and n = number of perovskite layers. Incorporation of ions with different sizes and charges in A, A′, and B sites can lead to a variety of compounds with unique behaviors. In, for example, the double-layered series $ALaNb_2O_7$ (A = alkali metal), Domen et al. has shown them to exhibit photocatalytic activity.[2] Sato et al. have also reported on ionic conductivity for $ALaNb_2O_7$ (A = Li, Na, K).[3] The triple-layered compound $KCa_2Nb_3O_{10}$ was found by Fukuoka and co-workers to exhibit superconductivity on doping with lithium.[4]

A further feature of ion-exchangeable layered perovskites is their ability to readily undergo topochemical reactions under relatively low temperatures (<500 °C). This chemistry can be used for the preparation of low temperature and metastable phases,[1] producing compounds typically not accessible by standard high temperature ceramic techniques. Reaction methods are varied and include ion exchange, intercalation, deintercalation, grafting, etc. One focus in this topochemistry has been the effort by some researchers to form metal–nonmetal layers within the perovskite hosts. This has resulted in the construction of both transition metal and alkali-metal halide arrays. The coexchange of cation and anion species for example can be used to build transition metal halide layers (e.g., Cu–Cl in $(CuCl)LaNb_2O_7$).[5] A three-step method involving ion exchange followed by reductive intercalation and oxidative deintercalation can lead to the formation of lithium chloride layers, $(Li_2Cl)LaNb_2O_7$.[6] Alkali-metal halide layers are also accessible by a two-step intercalation method; the reductive intercalation of $ALaNb_2O_7$ with rubidium or cesium can lead to $A_2LaNb_2O_7$, then oxidative intercalation of chloride ions from reaction with chlorine gas produces the alkali-metal halide A–Cl array $(A_2Cl)LaNb_2O_7$ (A = Rb, Cs).[7] Beyond metal halides, more recent efforts have resulted in the incorporation of other main-group anionic species; alkali-metal chalcogen layers can be formed with a similar two-step intercalation method where gaseous H_2Ch (Ch = S or Se) is used in the oxidative

Received: November 29, 2013
Published: January 10, 2014

   dx.doi.org/10.1021/ic402957c | Inorg. Chem. 2014, 53, 1773–1778

intercalation step to produce interlayer arrays containing the corresponding chalcogen hydride species.[8]

To further expand these strategies, our group has sought to develop methods that allow for the incorporation of oxygen into the various metal−nonmetal frameworks. Such methods could lead to new structurally interesting compounds with significant cooperative properties. Herein we report on an effective strategy for the incorporation of oxygen in the form of hydroxide ion. The approach utilizes a two-step reductive-oxidative method and results in the formation of new alkali-metal hydroxide arrays within double- and triple-layered niobate perovskites.

EXPERIMENTAL SECTION

Synthesis. *$ALaNb_2O_7$ (A = Li, Na, K, Rb, Cs) and $RbCa_2Nb_3O_{10}$.* Dion−Jacobson layered perovskites $ALaNb_2O_7$ and $RbCa_2Nb_3O_{10}$ were prepared by a simple solid state reaction.[2,9,10] La_2O_3 (Alfa Aesar, 99.99%) was preheated at 1000 °C for a day in order to remove any impurities as carbonates or hydroxides. Then, appropriate stoichiometric mixtures of La_2O_3, Nb_2O_5 (Alfa Aesar, 99.9985%), and $CaCO_3$ (Alfa Aesar, 99.99%) with a 25% excess of A_2CO_3 (A = K, Rb, Cs; K_2CO_3 Alfa Aesar 99.997%, Rb_2CO_3 Alfa Aesar 99%, Cs_2CO_3 Alfa Aesar 99.994%) were ground together and heated at 850 °C for 12 h and 1050 °C for 24 h with one intermediate grinding. The excess amount of A_2CO_3 was added to compensate for the volatilization of alkali-metal oxide components. The product was washed with distilled water and then dried at 110 °C for one day. $LiLaNb_2O_7$ and $NaLaNb_2O_7$ were prepared via ion exchange by reacting $ALaNb_2O_7$ (A = Rb or Cs) with molten salts of $LiNO_3$ (Alfa Aesar, 99.0% anhydrous) and $NaNO_3$ (Alfa Aesar, 99.999%) in a 1:10 molar ratio ($ALaNb_2O_7/ANO_3$) at 300 and 310 °C, respectively, for 4 days. All reactions produce white to off-white polycrystalline products.

$A_2LaNb_2O_7$ (A = Li, Na, K, Rb, Cs) and $Rb_2Ca_2Nb_3O_{10}$. $A_2LaNb_2O_7$ (A = Na, K, Rb, Cs) and $Rb_2Ca_2Nb_3O_{10}$ were all prepared by a reductive intercalation strategy similar to that reported by Armstrong and Anderson.[11] Pressed pellets of $ALaNb_2O_7$ and $RbCa_2Nb_3O_{10}$, formed by a simple hand press (7 mm dia), were placed inside a 13 mm Pyrex tube. A 10% molar excess of alkali-metal was weighed and placed inside a smaller Pyrex vial (9 mm). The vial was placed in the Pyrex tube, and the tube assembly was sealed under vacuum ($<10^{-4}$ Torr). The sealed tube was then heated at 310 °C (Na), 290 °C (K), 250 °C (Rb), or 290 °C (Cs) for 4 days.[7] To be sure that the sample was completely exposed to the alkali-metal vapor, the tube was rotated periodically. To remove excess alkali metal, the sample was then heated in a temperature gradient for an additional 3 days by keeping one end of the tube outside of the furnace. The final products, $A_2LaNb_2O_7$ and $Rb_2Ca_2Nb_3O_{10}$, have a dark blue-black color. $Li_2LaNb_2O_7$ was prepared from $LiLaNb_2O_7$ by reaction with an excess of n-BuLi (Aldrich, 2.5 M in hexane) in 1:10 molar ratio.[7] The reaction was carried out under inert atmosphere (Ar) with stirring for 4 days at room temperature. The product was washed several times with dry hexane to remove the excess lithium reagent. Note that $A_2LaNb_2O_7$ and $Rb_2Ca_2Nb_3O_{10}$ are air sensitive and were all stored and manipulated within an argon-filled drybox. All compounds readily deintercalate in air to form the starting materials ($ALaNb_2O_7$ and $RbCa_2Nb_3O_{10}$): $A_2LaNb_2O_7$ and $Rb_2Ca_2Nb_3O_{10}$ react immediately on exposure to moisture, changing from a dark blue-black color to white, typically within seconds. ***Caution!*** *Elemental alkali-metal reagents can explosively react with water and should therefore be handled and disposed with extreme care.*

$(A_2OH)LaNb_2O_7$ (A = K, Rb) and $(Rb_2OH)Ca_2Nb_3O_{10}$. Double- and triple-layer potassium- and rubidium-hydroxide perovskites were synthesized by oxidative intercalation with stoichiometric amounts of water vapor. Pressed pellets (*ca.* 0.5 g) of $A_2LaNb_2O_7$ and $Rb_2Ca_2Nb_3O_{10}$ were placed in a sealed evacuated tube with $CaC_2O_4\cdot H_2O$ (Sigma-Aldrich) at 200 °C for 2 days (Supporting Information Figure S1); setup is similar to that used in reductive intercalation. Water was generated from the decomposition of $CaC_2O_4\cdot H_2O$. The water content of calcium oxalate was confirmed by thermogravimetric analysis prior to use. Both the lithium and sodium compounds showed no obvious reaction under these conditions, while the cesium compound decomposed to the parent, $CsLaNb_2O_7$. Final products, $(A_2OH)LaNb_2O_7$ (A = K, Rb) and $(Rb_2OH)Ca_2Nb_3O_{10}$, are white in color. Products decompose to the parent compounds on exposure to air and were therefore stored and manipulated within an argon-filled drybox. The compounds appear slightly less reactive then the reduced intermediates, decomposing over several minutes.

$(Rb_2OD)LaNb_2O_7$. Deuterated samples, $(Rb_2OD)LaNb_2O_7$, were made by a method similar to that used for $(Rb_2OH)LaNb_2O_7$. Initially $CaC_2O_4\cdot H_2O$ was dehydrated by heating at 200 °C for 2 days. The sample was then reacted with deuterium oxide vapor (Sigma-Aldrich 100%, 99.96 atom % D) for 2 days at 65 °C. The resulting $CaC_2O_4\cdot D_2O$ was sealed in a Pyrex tube with a stoichiometric amount of $Rb_2LaNb_2O_7$ and heated for 2 days at 200 °C.

Characterization. X-ray powder diffraction (XRD) data were collected on a Philips X'Pert system equipped with Cu Kα radiation (λ = 1.5418 Å) and a curved graphite monochromator (diffracted beam side). Typical scans were collected in continuous mode with a scan rate of 0.02°/s. All air-sensitive samples were prepared inside an argon-filled glovebox; samples were mounted on an acrylic sample holder with silicon grease and sealed under polypropylene film. The peak positions and lattice parameters were refined by a least-squares method with the ChekCell program.[12] Crystal structures were refined by the Rietveld method with the GSAS software package.[13,14] In the case of the double layered perovskites, $(Rb_2Cl)LaNb_2O_7$[7] was used as a model for refinement, and for triple layered compounds, the model was derived from $RbCa_2Nb_3O_{10}$.[10] Infrared spectral analysis was carried out on a Perkin-Elmer System 2000 FT-IR. KBr salt plates were used for all hygroscopic samples where Parafilm and silicon grease were used to seal the air sensitive samples within pairs of plates.

Neutron diffraction data were collected on the POWGEN beamline at the Spallation Neutron Source (SNS) at Oak Ridge National Laboratory (ORNL).[15] Samples, sealed and transported in evacuated Pyrex tubes, were opened at ORNL in a glovebox containing helium and sealed in 6 mm diameter vanadium cans. The cans were loaded in a 24 sample changer, and room-temperature neutron diffraction data was collected using a frame of neutrons with a center wavelength of 1.5996 Å.

Elemental analysis was initially examined by energy dispersive spectroscopy (EDS) on a JEOL JSM 5410 scanning electron microscope equipped with an EDAX-DX Prime microanalytical system. Molar ratios were found to be approximately 2.5(2):1:1.83(9) Rb:La:Nb for $(Rb_2OH)LaNb_2O_7$ and 4.9(7):2.0(2):3.0(4) Rb:Ca:Nb for $(Rb_2OH)Ca_2Nb_3O_{10}$. The rubidium contents as determined by EDS for the series of compounds were unusually high; this is attributed to the air exposure and decomposition that occurs when samples are loaded in the SEM.[8] To complement EDS, a gravimetric approach was used for the water uptake by simply weighing samples before and after the oxidative intercalation step. In each case, 5 trials were used. For the compounds $(K_2OH)LaNb_2O_7$, $(Rb_2OH)LaNb_2O_7$, and $(Rb_2OH)Ca_2Nb_3O_{10}$ the average percent weight increase (theoretical shown parenthetically) was found to be 3.50 ± 0.47 (3.3), 2.98 ± 0.79 (2.8), and 3.10 ± 0.58 (2.5), respectively. The relatively large statistical errors in this analysis are primarily attributed to the small sample sizes.

RESULTS

Synthesis. Two-step topochemical reactions have been effectively used to make new alkali-metal hydroxide layered niobates. Initially alkali metal is intercalated into $ALaNb_2O_7$ to give the Ruddlesden−Popper related compound, $A_2LaNb_2O_7$ (eq 1).

$$ALaNb_2O_7 + A^0_{(g)} \rightarrow A_2LaNb_2O_7 \quad (1)$$

Water vapor, generated by the decomposition of calcium oxalate monohydrate at 200 °C (eq 2), is then used in the

dx.doi.org/10.1021/ic402957c | Inorg. Chem. 2014, 53, 1773−1778

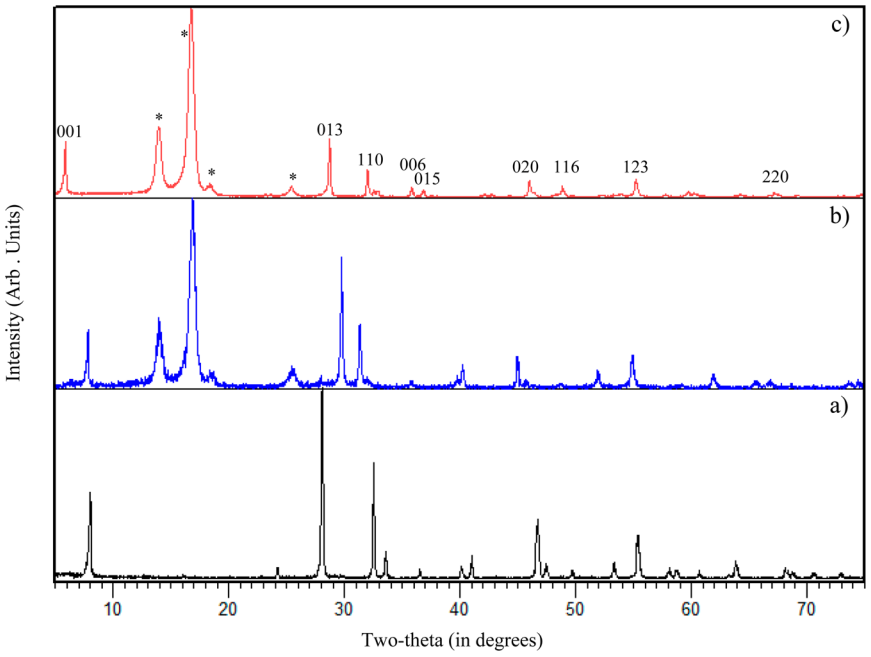

Figure 1. X-ray powder diffraction patterns for (a) $RbLaNb_2O_7$, (b) $Rb_2LaNb_2O_7$, (c) $(Rb_2OH)LaNb_2O_7$. Polypropylene film peaks are indicated by an asterisk (*). Indices for major reflections of $(Rb_2OH)LaNb_2O_7$ are included.

Table 1. Unit Cell Parameters for Series of Double- and Triple-Layered Perovskites Including Parents, Intermediates, and Hydroxide Products

compd	a (Å)	b (Å)	c (Å)	cell volume (Å^3)	layer spacing, L(Å)	ΔL relative to parent (Å)	ref
$KLaNb_2O_7$[a]	3.9060(1)	21.6030(7)	3.8879(1)	328.06	10.80		3
$K_2LaNb_2O_7$[a]	3.996(2)	21.49(1)	4.04(3)	346.899	10.74	−0.06	7
$(K_2OH)LaNb_2O_7$[b]	3.9183(5)		14.314(4)	219.77(1)	14.31	3.51	this work
$RbLaNb_2O_7$[a]	5.4941(1)	21.9901(1)	5.4925(4)	663.58	11.00		11
$Rb_2LaNb_2O_7$[a]	22.3096(1)	5.6975(1)	5.6937(1)	723.70	11.15	0.15	11
$(Rb_2OH)LaNb_2O_7$[b]	3.9303(1)		14.9624(9)	231.13(2)	14.96	3.96	this work
$(Rb_2OH)LaNb_2O_7$[b,c]	3.9132(1)		14.757(1)	225.97(1)	14.76	3.76	this work
$(Rb_2OD)LaNb_2O_7$[b,c]	3.9348(1)		14.7950(7)	229.07(2)	14.80	3.80	this work
$RbCa_2Nb_3O_{10}$[b]	3.8587(6)		14.9108(3)	222.01(1)	14.91		10
$Rb_2Ca_2Nb_3O_{10}$[b]	3.904(1)		15.2535(1)	232.03(4)	15.25	0.34	this work
$(Rb_2OH)Ca_2Nb_3O_{10}$[b]	3.8755(7)		18.856(5)	283.2(2)	18.86	3.95	this work

[a]Orthorhombic cell. [b]Tetragonal cell. [c]Neutron data.

oxidative intercalation reaction of the $A_2LaNb_2O_7$ phase (eq 3) to form the hydroxide.

$$CaC_2O_4\cdot H_2O(s) \xrightarrow{\Delta} CaC_2O_4(s) + H_2O(g) \quad (2)$$

$$A_2LaNb_2O_7 + H_2O(g) \rightarrow (A_2OH)LaNb_2O_7 + \frac{1}{2}H_2(g) \quad (3)$$

This synthetic approach works well for reactions with the double- and triple-layered compounds, $A_2LaNb_2O_7$ (A = K, Rb) and $Rb_2Ca_2Nb_3O_{10}$. In the case of $Cs_2LaNb_2O_7$, however, deintercalation occurred with the formation of the parent $CsLaNb_2O_7$ and $CsOH\cdot H_2O$. Both the lithium and sodium compounds, $A_2LaNb_2O_7$ (A = Li, Na), showed no evidence for reaction.

Structure. X-ray powder diffraction data for $(Rb_2OH)LaNb_2O_7$ is shown in Figure 1 relative to that of $RbLaNb_2O_7$ and $Rb_2LaNb_2O_7$. A clear expansion in the layer spacing can be seen with the shift of the 001 reflection to lower angles. $(Rb_2OH)LaNb_2O_7$ can be indexed on a tetragonal cell showing an increase in the c-parameter of almost 3 Å relative to the parent compound (Table 1). Similar behavior is seen as well in both $(K_2OH)LaNb_2O_7$ and $(Rb_2OH)Ca_2Nb_3O_{10}$ (Table 1, Supporting Information Figures S2−S3).

Rietveld Refinement on X-ray diffraction data started from a model similar to that used for $(Rb_2Cl)LaNb_2O_7$ with $P4/mmm$ space group[7] (Supporting Information). Neutron diffraction studies on $(Rb_2OD)LaNb_2O_7$ then allowed the inclusion of deuterium atoms in the model immediately adjacent to the interlayer oxygen (O4). The thermal parameter for O4 was found to be slightly large so other models were explored where this atom was located on a more general position. Various sites including (x, x, $^1/_2$), (x, y, $^1/_2$), and (x, y, z) were investigated, but all resulted in a significant increase in the tolerance factors relative to the 1d ($^1/_2$, $^1/_2$, $^1/_2$) site. In the case of deuterium, several sites were also investigated [(x, y, z), ($^1/_2$, $^1/_2$, z), and ($^1/_2$, y, $^1/_2$)]; the best fit was with deuterium disordered over the 4o site (x, $^1/_2$, $^1/_2$). The occupancy factors for La, Nb, and O1−O3 were all close to 1 and therefore fixed to 1 in the final refinements. Rb, O4, and D were found to be 1.057(2),

dx.doi.org/10.1021/ic402957c | Inorg. Chem. 2014, 53, 1773−1778

0.987(1), and 0.242(2), respectively. Observed, calculated, and difference plots for the refinement of $(Rb_2OD)LaNb_2O_7$ are shown in Figure 2. Crystallographic data and selected bond distances are presented in Tables 2 and 3, respectively.

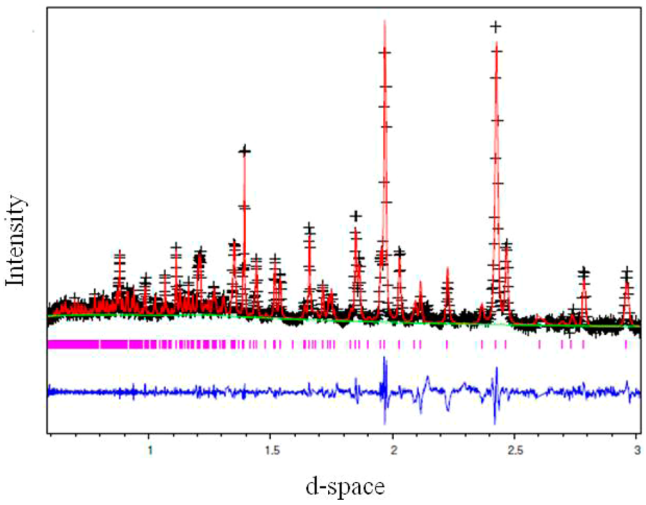

Figure 2. Rietveld refinement of $(Rb_2OD)LaNb_2O_7$ neutron diffraction data. Observed data are indicated by crosses, calculated pattern by a solid line (red), and the bottom curve (blue) is the difference plot. Reflection at ~2.2 Å is attributed to the vanadium sample holder. The green line is background.

Table 2. Neutron Diffraction Data for $(Rb_2OD)LaNb_2O_7$[a]

atom	site	x	y	z	U_{iso} (Å^2)	g
Rb	2g	0	0	0.3521(7)	0.019(2)	1.057(2)
La	1a	0	0	0	0.006(1)	1
Nb	2h	0.5	0.5	0.1490(6)	0.006(1)	1
O1	2h	0.5	0.5	0.2674(7)	0.041(3)	1
O2	1c	0.5	0.5	0	0.032(4)	1
O3	4i	0	0.5	0.1286(4)	0.018(1)	1
O4	1d	0.5	0.5	0.5	0.046(1)	0.987(1)
D	4o	0.24(1)	0.5	0.5	0.019(3)	0.242(2)

[a] $P4/mmm$, Z = 1, a = 3.9348(1) Å, c =14.7950(7) Å, V = 229.07(2) Å^3, R_p = 3.12%, R_{wp} = 2.83%, χ^2 = 4.298, and g = occupation factor.

Table 3. Selected Bond Lengths for $(Rb_2OD)LaNb_2O_7$

bond type	length (Å)
Rb−O_1 ×4	2.9954(1)
Rb−O_3 ×4	3.8006(2)
Rb−O_4 ×4	3.5873(1)
Nb−O_1 ×1	1.8212(1)
Nb−O_2 ×1	2.2025(1)
Nb−O_3 ×4	1.9934(1)
La−O_2 ×4	2.7812(1)
La−O_3 ×8	2.7222(1)
D−O_4 ×4	0.9837(1)

Vibrational Spectroscopy. Infrared spectroscopy verified the presence of OH^- and OD^- in the $(Rb_2OH)LaNb_2O_7$ and $(Rb_2OD)LaNb_2O_7$ compounds, respectively (Figure 3). The O−H stretch was observed at 3600 cm^{-1}. This is consistent with the literature where O−H stretches are in the range 3500−3600 cm^{-1}.[16] As expected, the O−D stretch, due to the greater mass of deuterium, was shifted to lower energies (2605 cm^{-1}). The ~1000 cm^{-1} shift in frequency is consistent with values seen for various alkali-metal hydroxides.[16] Though the deuterium sample was sealed in salt plates during analysis, after 24 h the spectrum shows evidence for water uptake with the appearance of the OH^- stretch (Figure 3d).

DISCUSSION

A two-step topochemical reaction strategy has been used to insert hydroxide ions into Dion−Jacobson-type layered perovskite hosts. Starting with a reductive intercalation procedure similar to that reported by Armstrong and Anderson,[11] we were able to prepare the $Rb_2LaNb_2O_7$ intermediate. Treatment with stoichiometric amounts of water then led to $(Rb_2OX)LaNb_2O_7$ (X = H, D). IR data showed clear evidence for both hydroxide and deuteroxide species in the products, respectively, and weight uptake and structure refinement data support the approximate composition of 2:1 for Rb:OH. This approach was successfully applied to both double- and triple-layered perovskites and is effective with potassium and rubidium compounds, but not lithium, sodium, or cesium. Similar topochemistry has been demonstrated for the insertion of chalcogen hydride species,[8] but unlike for the hydroxide, in the sulfur hydride system, the cesium analogue is accessible.[17] Though several factors could contribute to this difference in cesium reactivity, the less favorable size ratio in Cs:O (1.88/1.28) versus Cs:S (1.88/1.70) likely is a factor. (Size ratios are presented as relative crystallographic radii (Å) for coordination number (CN) = 8, except for sulfur CN = 6.)[18]

The structure of $(Rb_2OH)LaNb_2O_7$ (Figure 4) is similar to that of $(Rb_2Cl)LaNb_2O_7$.[7] Rubidium ions sit in cubic sites surrounded by 4 oxygens from the perovskite slab and the 4 hydroxide ions. The hydroxide oxygens are also cubically coordinated with respect to the rubidiums. In terms of the orientation of the O−H groups in $(Rb_2OH)LaNb_2O_7$, the hydrogens are disordered over a 4-fold site (x, $^1/_2$, $^1/_2$) within the x−y plane (Figure 5). The position is such that the hydrogen maximizes its distance from the set of four electrostatically repulsive rubidiums. The O−H bond distances are ~0.98 Å, in good agreement with literature values reported for hydroxides.[19,20] The hydrogens are oriented toward adjacent oxygens with distances to the next nearest (nn) oxygen being relatively large (D−O_{nn} = 2.94 Å).

This CsCl-like structural arrangement in $(Rb_2OH)LaNb_2O_7$ is interesting considering that the alkali-metal hydroxide, RbOD, is known to exist with lower coordination environments for the oxygens; below room temperature RbOD has a thallium-iodide-related structure (coordination number, CN = 5 + 2) and near room temperature, a rock-salt-related structure (CN = 6).[19,20] In $(Rb_2OH)LaNb_2O_7$, clearly the interlayer structure of this topochemically prepared compound is greatly influenced by the set of adjacent perovskite blocks. The interlayer environment leads to the stabilization of a higher coordination numbers (CN = 8) for both the alkali-metal and hydroxide ions. Also, in terms of hydrogen bonding, lower temperature RbOD (CN = 5 + 2) has a zigzag O−D···O motif (D−O_{nn} = 2.40 Å) while at higher temperatures, where CN = 6, this interaction dissipates (D−O_{nn} = 2.68 Å) allowing the OD groups to librate freely.[20] In comparison for $(Rb_2OH)LaNb_2O_7$, the D−O_{nn} are 2.94 Å so that hydrogen bonding is not expected to be significant. Figure 5 highlights the intermediate orientation of the deuteriums/hydrogens relative to the surrounding set of rubidiums.

The compounds $(K_2OH)LaNb_2O_7$ and $(Rb_2OH)LaNb_2O_7$ are isostructural (Figure 1 and Supporting Information Figure

dx.doi.org/10.1021/ic402957c | Inorg. Chem. 2014, 53, 1773−1778

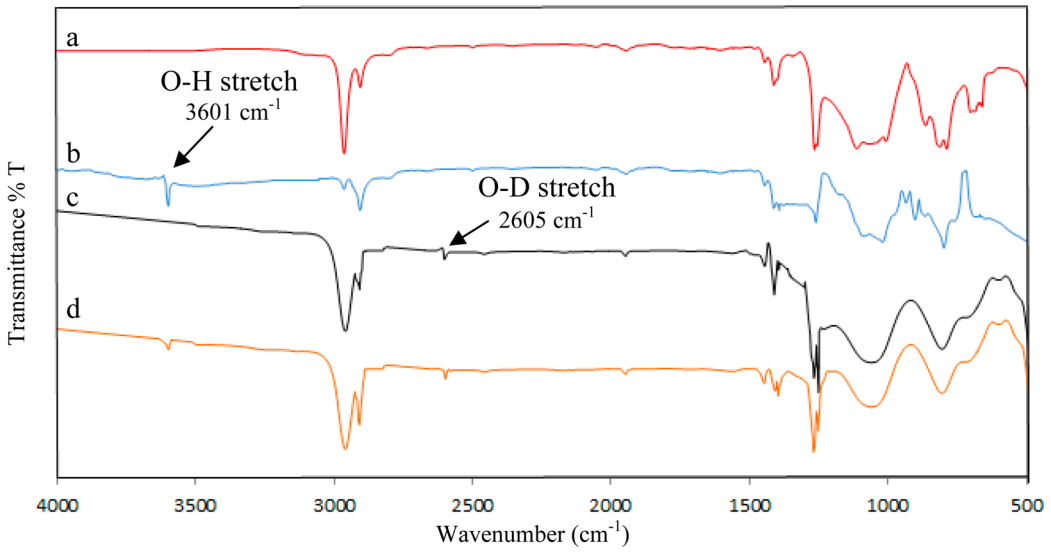

Figure 3. Infrared spectra of (a) $RbLaNb_2O_7$, (b) $(Rb_2OH)LaNb_2O_7$, (c) $(Rb_2OD)LaNb_2O_7$, and (d) $(Rb_2OD)LaNb_2O_7$ after 1 day in sealed salt plates.

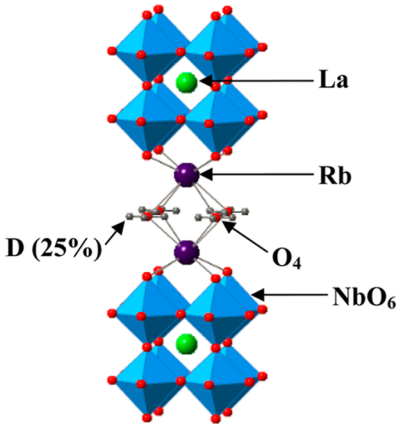

Figure 4. Crystal structure of $(Rb_2OD)LaNb_2O_7$ from neutron data. (Key: La = medium green spheres; oxygen = small red; NbO_6 octahedra = light blue; Rb = large dark purple; D = small gray.)

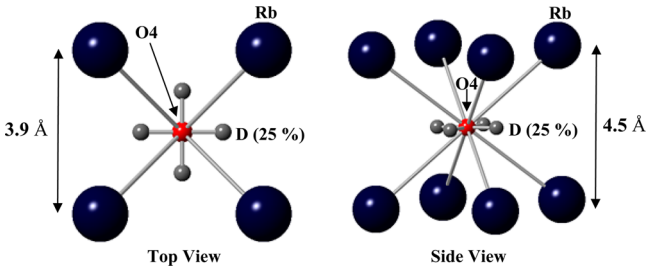

Figure 5. Local deuterium environment is shown. Top view (left) and side view (right) showing coordination of deuterium (gray), oxygen (red), and rubidium (dark blue).

S2). The slightly smaller layer expansion seen for the potassium compound (Table 1) is consistent with the smaller size of K (1.65 Å) relative to Rb (1.75 Å).[18] For the double-layered hydroxide $(Rb_2OH)LaNb_2O_7$ versus the triple-layered hydroxide $(Rb_2OH)Ca_2Nb_3O_{10}$, similar layer expansions are seen around 3.9 Å. It is noteworthy that the slight variation in layer expansion is seen in the X-ray data versus neutron: the X-ray *c*-parameter is about 0.2 Å larger than the neutron. We believe this to be an effect of a slight exposure of the X-ray sample to moisture during data collection; while the polymer film is effective in minimizing air exposure, it is not perfect, so the slight increase in *c* is associated with the additional uptake of water by $(Rb_2OH)LaNb_2O_7$. The handling of the neutron samples was such that they received no air exposure. Extended air exposure of samples of over 1−2 h leads to decomposition of product back to the parent compound.

There are several other known layered perovskites that contain hydroxide units. Pelloquin and co-workers have synthesized a series of transition metal double- and triple-layered perovskites that can reversibly take up hydroxide and water.[21] The compounds $Sr_3NdFe_3O_{7.5}(OH)_2$ and $Sr_3NdFe_3O_{7.5}(OH)_2{\cdot}H_2O$, for example, have been prepared by treating the anhydrous parent $Sr_3NdFe_3O_{8.5}$ with water at different temperatures. While the hydroxide units are located within the interlayer of the perovskite, the exact positions of the hydrogens were not determined. Other hydroxide-like units are seen in various perovskite solid acids. These compounds, often made by simple proton exchange of alkali metal cations within layered perovskites, also have hydroxide units. Examples here include $HLaNb_2O_7$, $HCa_2Nb_3O_{10}$, $H_2La_2Ti_3O_{10}$, and $HLaTiO_4$. In one detailed structure determination on deuterated samples of $HLaTiO_4$, Nishimoto and co-workers found the hydrogens were attached to apical oxygens within the interlayer and disordered over an 8-fold site.[22] The O−D bonds average about 0.971 Å and are oriented toward adjacent apical oxygens with $D{-}O_{nn}$ bond distances of about 2.054 Å. Similarly, Yip and Cussen studied the solid solution of $H_{1-x}Li_xTiO_4$ and observed comparable behavior.[23]

The two-step approach for the formation of alkali-metal hydroxide layers further expands the library of topochemical reactions available for the construction of metal−nonmetal layers within receptive layered perovskite hosts. Figure 6 highlights some of the compounds accessible so far through topochemical manipulation of $RbLaNb_2O_7$. Various combinations of ion exchange and/or intercalation can allow for the formation of either transition-metal or alkali-metal halides. Methods for inserting hydroxide anions represent the first among this series for inserting oxide species. This is significant in that many oxides of perovskites can show technologically

dx.doi.org/10.1021/ic402957c | Inorg. Chem. 2014, 53, 1773−1778

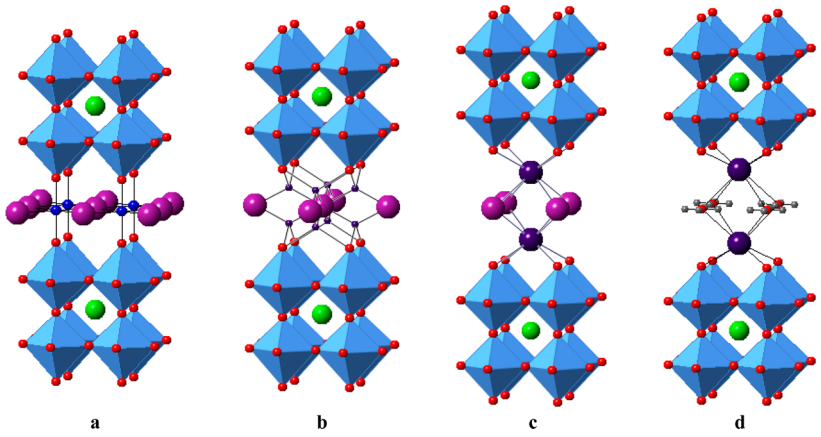

Figure 6. Various structures accessible topochemically within layered perovskite hosts. (a) $(MCl)LaNb_2O_7$ (M = transition metal), (b) $(Li_2Cl)LaNb_2O_7$, (c) $(Rb_2Cl)LaNb_2O_7$, and (d) $(Rb_2OH)LaNb_2O_7$. (Key: M = small blue spheres; Cl = large violet; La = medium green; oxygen = small red; NbO_6 octahedra = light blue; Li = small dark purple; Rb = large dark purple; H/D = gray.)

important cooperative phenomena.[24] Should one be able to further expand this approach to direct the coinsertion of transition metals and oxides species, these topochemical strategies become especially pertinent.

■ ASSOCIATED CONTENT

Ⓢ Supporting Information

Figure of reaction setup for intercalation, X-ray powder patterns for $(K_2OH)LaNb_2O_7$ and $(Rb_2OH)Ca_2Nb_3O_{10}$, and Rietveld refinements of $(Rb_2OH)LaNb_2O_7$ from X-ray and neutron data. This material is available free of charge via the Internet at http://pubs.acs.org.

■ AUTHOR INFORMATION

Corresponding Author

*E-mail: jwiley@uno.edu.

Notes

The authors declare no competing financial interest.

■ ACKNOWLEDGMENTS

Support from the National Science Foundation (DMR-1005856) is gratefully acknowledged. Part of the research conducted at ORNL's Spallation Neutron Source was sponsored by the Scientific User Facilities Division, Office of Basic Energy Sciences, U.S. Department of Energy.

■ REFERENCES

(1) Ranmohotti, K. G. S.; Josepha, E.; Choi, J.; Zhang, J.; Wiley, J. B. *Adv. Mater.* **2011**, *23*, 442−460.
(2) Domen, K.; Kondo, J. N.; Hara, M.; Takata, T. *Bull. Chem. Soc. Jpn.* **2000**, *73*, 1307−1331.
(3) Sato, M.; Abo, J.; Jin, T.; Ohta, M. *J. Alloys Compd.* **1993**, *192*, 81−83.
(4) Fukuoka, H.; Isami, T.; Yamanaka, S. *Chem. Lett.* **1997**, 703−704.
(5) Viciu, L.; Caruntu, G.; Royant, N.; Koenig, J.; Zhou, W. L.; Kodenkandath, T. A.; Wiley, J. B. *Inorg. Chem.* **2002**, *41*, 3385−3388.
(6) Viciu, L.; Kodenkandath, T. A.; Wiley, J. B. *J. Solid State Chem.* **2007**, *180*, 583−588.
(7) Choi, J.; Zhang, X.; Wiley, J. B. *Inorg. Chem.* **2009**, *48*, 4811−4816.
(8) Ranmohotti, K. G. S.; Montasserasadi, M. D.; Choi, J.; Yao, Y.; Mohanty, D.; Josepha, E.; Adireddy, S.; Caruntu, G.; Wiley, J. B. *Mater. Res. Bull.* **2012**, *47*, 1289−1294.
(9) Kumada, N.; Kinomura, N.; Sleight, A. W. *Acta Crystallogr.* **1996**, *C52*, 1063−1065.
(10) Liang, Z. H.; Tang, K. B.; Chen, Q. W.; Zheng, H. G. *Acta Crystallogr.* **2009**, *E65*, i44.
(11) Armstrong, A. R.; Anderson, P. A. *Inorg. Chem.* **1994**, *33*, 4366−4369.
(12) Laugier, J.; Bochu, B. *ChekCell*; Domaine Universitaire: Saint Martin d'Hères, France; http://www.inpg.fr/LMGP.
(13) Larson, A. C.; Von Dreele, R. B. *General Structure Analysis System (GSAS)*; Report LAUR 86-748; Los Alamos National Laboratory: Los Alamos, NM, 2000.
(14) Toby, B. H. *J. Appl. Crystallogr.* **2001**, *34*, 210−213.
(15) Huq, A.; Hodges, J. P.; Gourdon, O.; Heroux, L. *Z. Kristallogr. Proc.* **2011**, *1*, 127−135.
(16) Gennick, I.; Harmon, K. M. *Inorg. Chem.* **1975**, *14*, 2214−2219.
(17) Montasserasadi, M. D.; Wiley, J. B. Work in progress.
(18) Shannon, R. D. *Acta Crystallogr.* **1973**, *A32*, 751−767.
(19) Jacobs, H.; Kockelkorn, J.; Tacke, Th. *Z. Anorg. Allg. Chem.* **1985**, *531*, 119−124.
(20) Jacobs, H.; Mach, B.; Lutz, H.-D.; Henning, J. *Z. Anorg. Allg. Chem.* **1987**, *544*, 28−54.
(21) Pelloquin, D.; Hadermann, J.; Giot, M.; Caignaert, V.; Michel, C.; Hervieu, M.; Raveau, B. *Chem. Mater.* **2004**, *16* (9), 1715−1724.
(22) Nishimoto, S.; Matsuda, M.; Harjo, S.; Hoshikawa, A.; Kamiyama, T.; Ishigaki, T.; Miyake, M. *J. Eur. Ceram. Soc.* **2006**, *26* (4−5), 725−729.
(23) Yip, T. W. S.; Cussen, E. J. *Inorg. Chem.* **2013**, *52*, 6985−6993.
(24) Rao, C. N. R.; Raveau, B. *Transition Metal Oxides—Structure, Properties, and Synthesis of Ceramic Oxides*, 2nd ed.; Wiley-VCH: New York, 1998.